Prepared for submission to JCAP

Cosmic ray mass composition at the *knee* using azimuthal fluctuations of air shower particles detected at ground by the KASCADE experiment

N. Arsene

Institute of Space Science,
P.O.Box MG-23, Ro 077125 Bucharest-Magurele, Romania

E-mail: nicusorarsene@spacescience.ro

Abstract. The presence of hadronic sub-showers causes azimuthal non-uniformity in the particle distributions on the ground in vertical air showers. The LCm parameter, which quantifies the non-uniformity of the signal recorded in detectors located at a given distance on a ring around the shower axis, has been successfully introduced as a gamma/hadron discriminator at PeV energies [25]. In this work, we demonstrate that the LCm parameter can effectively serve as a mass composition discriminator in experiments that employ a compact array of detectors, like KASCADE. We reconstruct the LCm parameter distributions in the energy range $\lg(E/\text{eV}) = [15.0 - 16.0]$ using measurements from the KASCADE experiment, with intervals of $\lg(E/\text{eV}) = 0.1$, which are then fitted with MC templates for five primary nuclei species p, He, C, Si, and Fe considering five hadronic interaction models: QGSjet-II-02, QGSjet-II-04, EPOS-LHC, SIBYLL 2.3c and SIBYLL 2.3d. We find that the LCm parameter exhibits minimal dependence on the specific hadronic interaction model considered. The reconstructed fractions of individual species demonstrate a linear decrease in the abundance of protons with increasing energy, while the heavier components become prevalent above the *knee* as predicted by all five hadronic interaction models. Our findings indicate that the abundance of particle types as a function of energy aligns with three astrophysical models that link the *knee* to the acceleration and propagation of cosmic rays within the Galaxy. These findings suggest that the LCm parameter could be a valuable tool for forthcoming measurements of the LHAASO experiment to enhance our knowledge about the origin and acceleration mechanisms of cosmic rays.

Contents

1 Introduction

Various ground-based experiments have measured the energy spectrum of cosmic rays for several decades. To understand their origin and acceleration mechanisms, it is essential to accurately determine the mass composition of the cosmic rays, as well as their arrival directions, and correlate these measurements with a precise picture of the galactic/extragalactic magnetic fields. The experimental measurements reveal some remarkable structures in the flux of the primary cosmic rays ($dN/dE \propto E^{\gamma}$): a change of the spectral index γ from -2.7 to -3.1 around $E \sim 4 \times 10^{15}$ eV (the *knee*) [1–8], a change from $\gamma = -2.95$ to $\gamma = -3.24$ at $E \sim 8 \times 10^{16}$ eV (the *second knee*) [9–11] and a flattening in the spectrum at $E \sim 5 \times 10^{18}$ eV (the *ankle*) where the γ index changes from -3.29 to -2.51 [12–15].

Different scenarios have been proposed to explain the appearance of the *knee* in the energy spectrum. The most widely considered suggest that the *knee* is due to the maximum energy that can be reached by cosmic rays accelerated in supernova remnants e.g. [16, 43, 45], or it is due to the effects of cosmic ray propagation through the interstellar medium e.g. [17, 44]. Another class of models explain the *knee* as a consequence of the interaction of cosmic rays with the photon fields [18]. A detailed description of these models compared with direct and indirect measurements of cosmic rays properties around the *knee* is given in [19].

Measurements of the mass composition around the *knee* indicate an increase in the mean logaritmic mass ($\ln A$) with increasing energy of the primary cosmic rays, which suggests that individual elements may be undergoing sequential cut-offs [1, 22–24]. However, an accurate interpretation of the results is limited by discrepancies between the considered hadronic interaction models.

Significant findings were recently achieved through the detection of gamma rays with energies in the PeV range [20, 21]. Their arrival direction correlated with a better knowledge about mass composition of cosmic rays around the *knee* can significantly enhance our understanding about their acceleration sources.

In this work, we present a new mass composition reconstruction method that utilizes the non-uniformity of the signal recorded in detectors located at a fixed distance on a ring around the shower axis at ground level. Originally introduced as a gamma/hadron discrimination technique at PeV energies [25], we demonstrate that this method shows minimal dependence on the specific hadronic interaction model and can effectively serve as mass composition

discriminator in cosmic ray experiments with a relatively compact array of detectors, such as KASCADE [40].

The paper is organized as follows: in Section 2 we introduce the LCm parameter which is used as mass discriminator at PeV energies, in Section 3 we describe how the Monte Carlo (MC) simulations were obtained, in Section 4 we reconstruct the distributions of LCm from KASCADE data [33], in Section 5 we perform the mass composition reconstruction in the energy range $\lg(E/\mathrm{eV}) = [15.0 - 16.0]$ on the basis of five hadronic interaction models and compare the results with predictions of three astrophysical models of the *ankle*. Section 6 concludes the paper.

2 The LCm observable

The stochastic nature of the extensive air showers (EAS) development in Earth's atmosphere produces non-uniformity in particle densities at ground level. In vertical showers, we would expect similar densities of secondary particles at a fixed distance around the shower core. Neglecting the influence of the geomagnetic field, the presence of hadronic sub-showers can distort this symmetry. At the same energy, a gamma-induced shower will present a less complex structure of particle densities on the ground than a proton-induced shower. This is because the development of gamma showers is mainly driven by electromagnetic interactions. In the same context, we expect larger fluctuations in the azimuthal signal in proton-induced showers compared to iron showers due to the larger fluctuations in primary interaction heights in the atmosphere. To account for such non-uniformity in the signal induced in detectors at a given distance from the shower axis, the LCm parameter was introduced as a promising gamma/hadron discriminator [25].

The LCm parameter is computed as $LCm = \log(C_k)$, where the C_k variable is defined for each radial ring k around the shower core at ground as [25]:

$$C_k = \frac{2}{n_k(n_k-1)} \frac{1}{\langle S_k \rangle} \sum_{i=1}^{n_k-1} \sum_{j=i+1}^{n_k} (S_{ik} - S_{jk})^2, \tag{2.1}$$

where n_k represents the number of detectors in ring k, $\langle S_k \rangle$ is the mean signal registered in the detectors of the ring k, while S_{ik} and S_{jk} stand for the signals in the detectors i and j of the ring k, respectively. The term $\frac{2}{n_k(n_k-1)}$ accounts for the inverse of the number of two-combinations for n_k detectors, $\binom{n_k}{2}$. A greater non-uniformity in the azimuthal distribution of the signal results in an increased value of the C_k variable. In contrast, a perfectly uniform azimuthal distribution results in C_k approaching zero.

The value of LCm parameter depends on the primary energy and the fill factor (FF) of the detectors array. For a fixed primary energy, the value of LCm parameter as a function of radial range is roughly constant above $\gtrsim 40$ m up to 1000 m. In this analysis we reconstruct the LCm parameter for both data and simulations in the energy range $\lg(E/\mathrm{eV}) = [15.0 - 16.0]$ in intervals of $\lg(E/\mathrm{eV}) = 0.1$, considering the radial range $r_k = [100 - 110]$ m. The following section will explain the methodology used to generate simulation sets for five primary species, namely p, He, C, Si, and Fe, using various hadronic interaction models. The simulation sets were then used to construct LCm distributions in each energy interval, which are then used in determining the mass composition of cosmic rays using data collected by the KASCADE experiment.

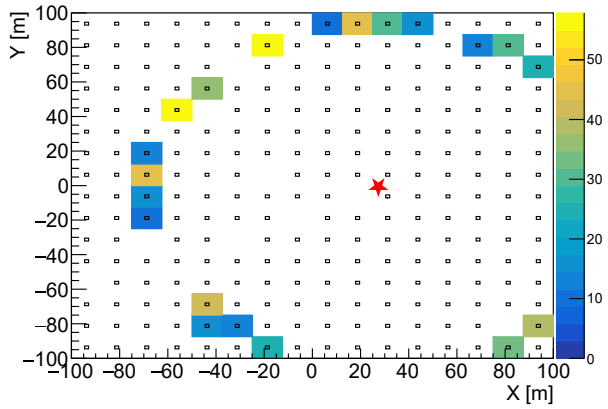

Figure 1. Visualization of the 252-detector array of the KASCADE experiment. The color gradient represents the energy deposited in [MeV] by the electromagnetic component in e/γ-detectors located in the radial range r_k = [100 - 110] m from the shower core position indicated by the red star. The reconstructed parameters of this event with the internal KASCADE counting number 302724 are: the primary energy $\lg(E/\mathrm{eV}) = 15.6$, the zenith angle of the shower axis $\theta = 12.1°$ and the azimuth angle $\phi = 53.7°$.

3 LCm distributions from Monte Carlo simulations of KASCADE array

The KASCADE experiment utilized a detector array consisting of 252 stations arranged on a rectangular grid with a 13 m spacing covering an area of 200×200 m^2, being able to reconstruct the properties of extensive air showers with energies in the range $\lg(E/\mathrm{eV}) = [14 - 17]$. The stations were equipped with both shielded and unshielded detectors, allowing for the simultaneous and independent measurement of the electromagnetic and muonic components from extensive air showers. Above a 3 MeV threshold, the liquid scintillation counters located above the shielding were used to detect the charged component of the shower's secondary particles. The muonic component was measured by utilizing 3.2 m^2 of plastic scintillators that were placed beneath lead and iron absorber sheets [40]. In Figure 1 we represent the layout of 252-detector array of the KASCADE experiment together with the energy deposited by the electromagnetic component in e/γ-detectors located at r_k = [100 - 110] m from the shower axis, from the event with the internal counting number 302724, with the primary energy $\lg(E/\mathrm{eV}) = 15.6$, zenith angle of the shower axis $\theta = 12.1°$ and the azimuth angle $\phi = 53.7°$.

The MC simulations of extensive air showers for KASCADE experiment is a three-step procedure [29, 33]. The development of showers in the atmosphere is simulated with CORSIKA [30, 31], the signal / energy deposit in the KASCADE detectors is simulated with CRES package based on GEANT3 [32] while the reconstruction of the air shower observables like primary energy, arrival direction, the number of electrons / muons / hadrons and so on, is performed with the KRETA package. It should be noted that the KRETA package, which follows the same procedures, is utilized for reconstructing the events that were recorded by KASCADE experiment.

Five hadronic interaction models at high energies were considered: EPOS-LHC [35], QGSjet-II-02, QGSjet-II-04 [34], SIBYLL 2.3c [36] and SIBYLL 2.3d [37], while the low

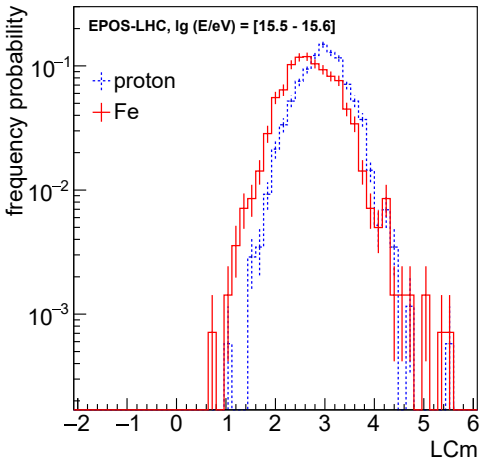

Figure 2. The LCm distributions for proton induced showers *(dashed blue)* and Fe induced showers *(continuous red)* in the energy interval $\lg(E/\text{eV}) = [15.5 - 15.6]$ on the basis of EPOS-LHC and FLUKA as hadronic interaction models at high and low energies, respectively.

energy hadronic interactions ($E_{\text{lab}} < 200$ GeV) were modeled with FLUKA [38]. Five species of primary particles were simulated (p, He, C, Si, and Fe) in the energy range $\lg(E/\text{eV}) = [15.0 - 16.0]$ with intervals of $\lg(E/\text{eV}) = 0.1$ considering the energy spectral index $\gamma = -2.7$. The zenith angles of the shower axis were isotropically sampled from the range $\theta = [0° - 20°]$ and the azimuthal distribution was uniformly sampled in the range $\phi = [0° - 360°]$. The statistics in the simulation sets is of the order of 10^3 - 10^4 events / primary species / model in each energy interval.

For each primary species, hadronic interaction model and energy interval we build LCm distributions using Equation 2.1 where the signal S_i represents the energy deposit of the electromagnetic component in the "i" e/γ-detector from the radial interval $r_k = [100 - 110]$ m around the shower core position. This quantity is separately and independent measured by the muonic and hadronic energy deposited in KASCADE detectors. In Figure 2 are represented the LCm distributions reconstructed for proton and Fe induced showers based on EPOS-LHC hadronic interaction model in the energy interval $\lg(E/\text{eV}) = [15.5 - 15.6]$. The shapes of the two distributions are distinct, as well as their mean and dispersion values. The larger LCm values for proton induced showers are due to the larger fluctuations in the heights of the first interaction points in the atmosphere.

A very important aspect of the LCm parameter is that it does not depend on the specific hadronic interaction model used in the simulation process of the extensive air showers. Therefore, using experimental data obtained from the KASCADE experiment, the mass composition of cosmic rays can be determined in a model-independent way. In Figure 3 we represent the LCm distributions in the energy bin $\lg(E/\text{eV}) = [15.5 - 15.6]$ for proton and Fe induced showers, as predicted by all hadronic interaction models considered in this analysis. It is evident that the models show a remarkable level of agreement. The same degree of compatibility is obtained on the entire energy spectrum analyzed in this paper $\lg(E/\text{eV}) = [15.0 - 16.0]$. Figure 4 provides an example of the quantitative agreement between LCm distributions that are predicted by different models. We compare the LCm distribu-

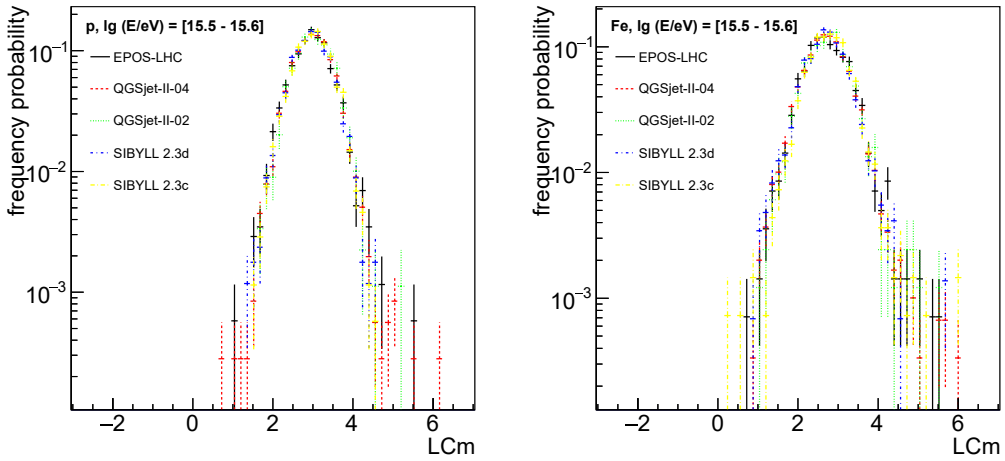

Figure 3. The *LCm* distributions for proton *(left)* and Fe *(right)* in the energy interval $\lg(E/\mathrm{eV}) = [15.5 - 15.6]$ as predicted by all five hadronic interaction models considered in this work.

tions obtained for proton-induced showers with EPOS-LHC and QGSjet-II-04 in three energy intervals: $\lg(E/\mathrm{eV}) = [15.1 - 15.0]$, $\lg(E/\mathrm{eV}) = [15.5 - 15.6]$ and $\lg(E/\mathrm{eV}) = [15.8 - 15.9]$. The comparison is made by computing the ratio of the two distributions. The values of the *ratio* parameter displayed at the bottom of the plots are very close to 1 throughout the distribution, within the limits of statistical uncertainties. The model-independence of the *LCm* distributions for heavier nuclei is at least as good as it is for proton-induced showers. Using

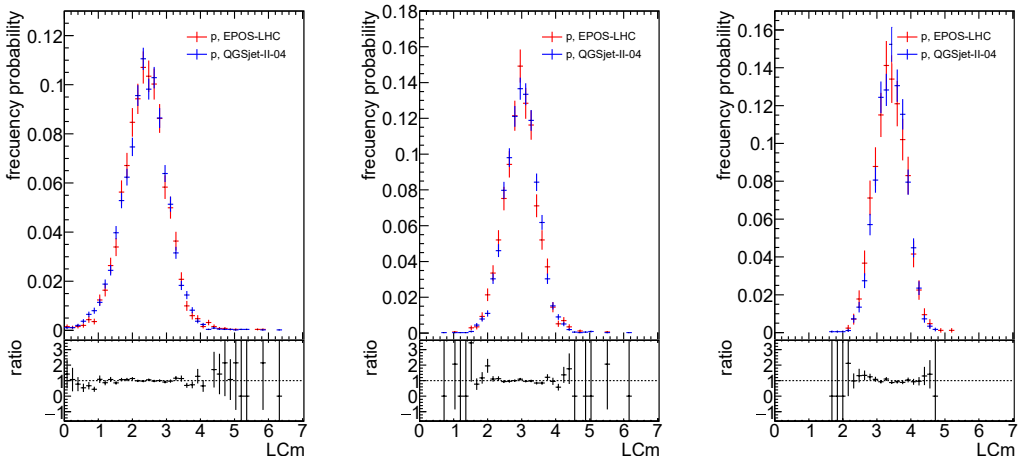

Figure 4. The *LCm* distributions obtained for proton-induced showers with EPOS-LHC *(red)* and QGSjet-II-04 *(blue)* in three energy intervals $\lg(E/\mathrm{eV}) = [15.1 - 15.2]$ *(left)*, $\lg(E/\mathrm{eV}) = [15.5 - 15.6]$ *(middle)* and $\lg(E/\mathrm{eV}) = [15.8 - 15.9]$ *(right)*. The ratio of the distributions is displayed on the bottom of each plot.

these distributions, we will perform a mass composition analysis by fitting the experimental

LCm distributions for each energy interval with MC templates for five primary species (p, He, C, Si and Fe) in Section 5.

4 LCm distributions from KASCADE data

Our analysis focused on the experimental data collected by KASCADE from 1996 until the end of its final operation in 2013 [33]. Specifically, we considered data within the energy range $\lg(E/\text{eV}) = [15.0 - 16.0]$ and restricted our analysis to vertical showers, i.e., those with a zenith angle θ in the range of $[0° - 20°]$. This was done to prevent potential biases in the azimuthal distribution of the signal resulting from attenuation and geometric effects [39].

In the initial analysis using the KRETA reconstruction program, the collaboration applied the "Data Selection Cuts KASCADE" to the data [28]. These cuts are deemed essential by the collaboration to ensure a consistent level of quality in the published data sets. These cuts consist in: a successful reconstruction process of the event in the KASCADE Array Processor, the KASCADE Array has produced a trigger signal, no more than 2 out of the 16 Array clusters to be missing, the reconstructed shower core is within a 91 m radius around the centre of the KASCADE array, the lateral shower shape parameter s has to be in the range $s = [0.1 - 1.48]$, the zenith angle of the shower axis is $\theta < 60°$, the number of electrons $N_e > 100$ and the number of muons $N_\mu > 100$. More stringent cuts are highly recommended by the KASCADE collaboration, which we took into account both in data and simulation reconstruction procedures. These cuts impose $\theta < 42°$, $s = [0.6 - 1.3]$ and $N_e > 100000$. Important to mention that the e/γ-detectors of the KASCADE array reach the full efficiency at $\lg(N_e) > 4.25$, therefore, no biases are expected in the reconstruction process of the LCm parameter.

In Figure 5, we present the LCm distributions in each energy interval within the range of $\lg(E/\text{eV}) = [15.0 - 16.0]$ reconstructed from KASCADE data. We have applied the aforementioned cuts and only the events that have passed the reconstruction procedure are included. The number of surviving events N is indicated on the plots for each energy interval of $\lg(E/\text{eV}) = 0.1$. As can be seen, the mean of the LCm distributions increases with increasing primary energy, and the spread of the distributions become narrower as the primary energy increases. In the upcoming section, we will use the MC predictions derived in Section 3 to fit the experimental LCm distributions. This will enable us to investigate the dependence of the individual abundance of primary nuclei on primary energy within the energy range of $\lg(E/\text{eV}) = [15.0 - 16.0]$.

5 Mass composition around the *knee*

In this study, we utilized KASCADE data to construct experimental LCm distributions and compared them with MC predictions for five primary species (p, He, C, Si, and Fe) using five different hadronic interaction models (QGSjet-II-02, QGSjet-II-04, EPOS-LHC, SIBYLL 2.3c and SIBYLL 2.3d). We employed a Chi-Square minimization method to fit the experimental distributions, and we calculated the parameter errors using the Minos technique.

In Figure 6, we present an example of an LCm distribution reconstructed from KASCADE data in the energy interval $\lg(E/\text{eV}) = [15.6 - 15.7]$, along with the individual fractions of nuclei that best describe the observed distribution as predicted by the QGSjet-II-04 *(left)* and EPOS-LHC *(right)* hadronic interaction models. Since we have observed from simulations that the LCm parameter shows minimal dependence on the choice of the hadronic interaction

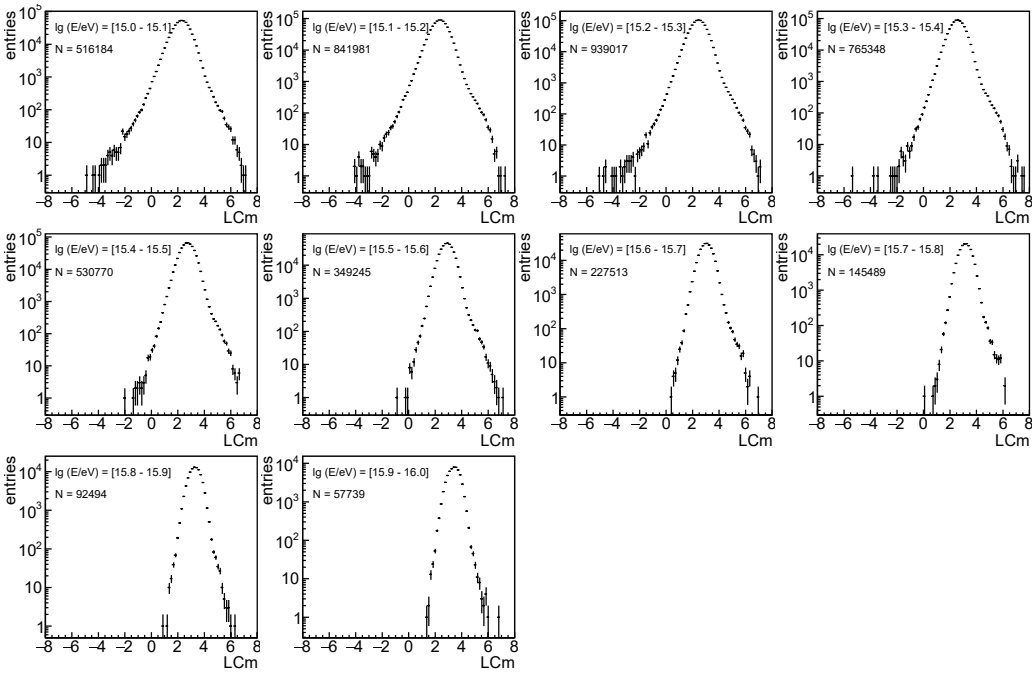

Figure 5. The LCm distributions reconstructed from KASCADE data in each energy interval in the range $\lg(E/\mathrm{eV}) = [15.0 - 16.0]$. The number of events N that survived all applied cuts is indicated on each plot.

model, the obtained individual fractions of elements are in very good agreement. The lack of simulated distribution tails observed in Figure 6, resulting from small statistics compared to experimental data, cannot significantly influence the result of the fit.

To evaluate the fit quality in each energy interval we considered the Kolmogorov-Smirnov (KS) test which is a valuable tool for evaluating the goodness of fit in statistical modeling, particularly when the size of the data set is relatively large. This test is based on the comparison of the cumulative distribution function (CDF) of the fitted model with the observed data, which allows for a more comprehensive assessment of the agreement between the model and the data than other methods like the Chi-Squared test. Moreover, the KS test does not depend on the binning of the data or the model, making it more robust and reliable when working with limited statistics. A high KS probability indicates that the fitted model is a good match to the data, which means that the overall shape of the histograms of the two are very similar. The goodness-of-fit parameters (KS probability) evaluated for each energy interval and hadronic interaction model are listed in Table 1 and suggest, with few exceptions, an excellent agreement between data and all models on the entire energy range considered in this work.

The evolution of the individual fractions of nuclei as a function of primary energy in the range $\lg(E/\mathrm{eV}) = [15.0 - 16.0]$ reconstructed on the basis of LCm observable is represented in Figure 7 for all five hadronic interaction models considered. One key point to note from these results is that all five hadronic interaction models indicate a similar trend in the individual abundance of each primary species with increasing energy. Additionally, the evolution of

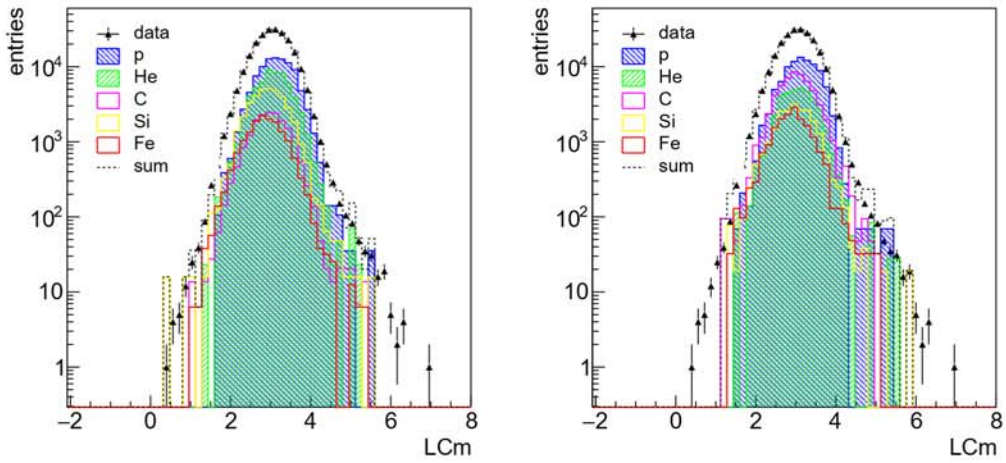

Figure 6. *LCm* distribution reconstructed from KASCADE data in the energy interval $\lg(E/\mathrm{eV}) = [15.6 - 15.7]$ *(black triangles)*. The reconstructed fractions of each element (p, He, C, Si and Fe) are displayed on each plot. The *(dashed line)* represents their sum as predicted by QGSjet-II-04 *(left)* and EPOS-LHC *(right)*.

$\lg(E/\mathrm{eV})$	15.05	15.15	15.25	15.35	15.45	15.55	15.65	15.75	15.85	15.95
EPOS-LHC	0.99	0.99	0.98	0.98	0.79	0.89	1.00	0.74	1.00	0.94
QGSjet-II-02	0.86	1.00	0.97	0.95	1.00	0.89	0.99	0.99	0.35	0.66
QGSjet-II-04	0.17	0.14	< 0.1	0.19	0.59	0.89	1.00	0.76	0.97	0.71
SIBYLL 2.3c	< 0.1	< 0.1	0.96	1.00	0.69	0.92	0.97	0.80	0.94	0.88
SIBYLL 2.3d	0.77	< 0.1	0.98	0.97	0.77	0.43	0.98	1.00	0.95	1.00

Table 1. The KS probability as goodness-of-fit obtained after the comparison of the data with the fitted model. The values of $\lg(E/\mathrm{eV})$ correspond to the center of each energy interval.

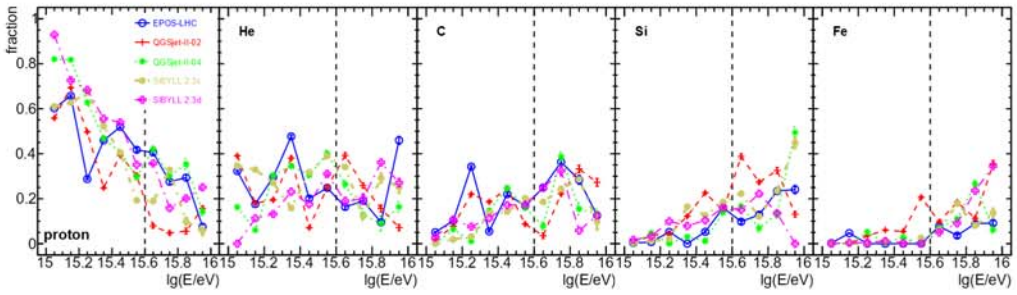

Figure 7. The evolution of individual fractions of nuclei (p, He, C, Si and Fe) as a function of primary energy in the range $\lg(E/\mathrm{eV}) = [15.6 - 15.7]$ as predicted by all five hadronic interaction models considered in this work. The parameter errors are typically smaller than the points size.

the individual fractions of nuclei with energy is highly consistent with previous studies that relied on different observables obtained from extensive air showers [23, 42]. These findings

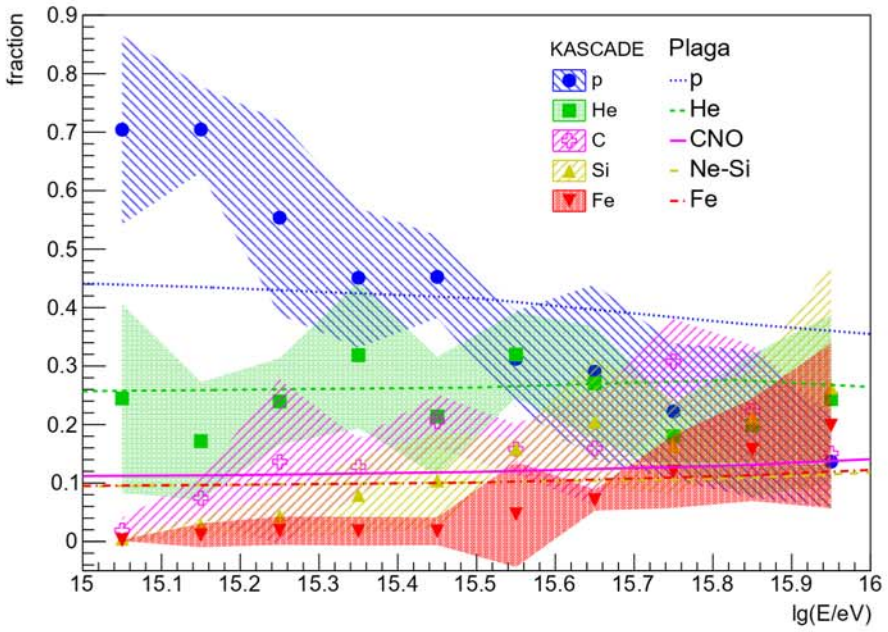

Figure 8. Evolution of the individual fractions of nuclei obtained in this work as a function of primary energy, in comparison with predictions of the astrophysical model proposed by Plaga [43]. The error bands represent the standard deviation of the individual fractions obtained from all five hadronic interaction models used in this work.

underscore the discriminative potential of the LCm parameter for determining the mass composition of cosmic rays in experiments that use a relatively compact array of detectors e.g. [41].

We compare the mass composition obtained in this analysis with three astrophysical models that attempt to explain the origin of the *knee* in the energy spectrum as a consequence of different acceleration and propagation scenarios. We use the averaged fractions of each primary species predicted by all five hadronic interaction models as a function of energy. In Figure 8, we show the evolution of the averaged fraction of individual species obtained in this work, in comparison with the predictions of the astrophysical model of the *knee* proposed by Plaga [43]. The model considers that cosmic rays are accelerated by "cannonballs" ejected in supernova explosions. The second astrophysical model considered for comparison was proposed by Sveshnikova in [45] and relate the presence of the *knee* as a consequence of the maximum energy attained by cosmic rays in shock fronts of supernova explosions. The comparison of this model with the data obtained in this work is represented in Figure 9. The third model used for coparison with the data was proposed by Swordy [44] and assume that the *knee* is related to the leakage of cosmic rays from the Galaxy during propagation process. The comparison is displayed in Figure 10.

The mass composition around the *knee* obtained from KASCADE data using the LCm parameter displays a substantial level of agreement with these three astrophysical models in regards to the evolutionary trend of primary abundance of different particle types as a

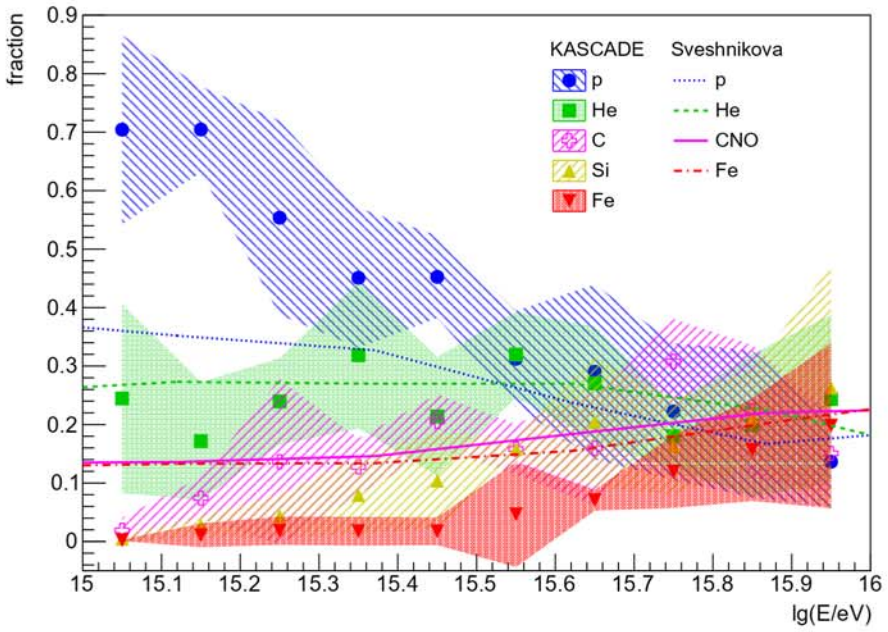

Figure 9. Evolution of the individual fractions of nuclei obtained in this work as a function of primary energy, in comparison with predictions of the astrophysical model proposed by Sveshnikova [45]. The error bands represent the standard deviation of the individual fractions obtained from all five hadronic interaction models used in this work.

function of energy. Notably, the model proposed by Plaga shows a remarkable agreement, with the relative abundances of individual species matching perfectly those derived from our analysis.

Based on the experimental capabilities of the LHAASO square kilometer array (KM2A) experiment [46, 47], which includes 5249 electromagnetic detectors spaced at 15 meters and 1188 muon detectors spaced at 30 meters, we can conclude that the method proposed in this study is a suitable tool for reconstructing the mass composition around the knee from the forthcoming measurements of the LHAASO experiment.

6 Summary and Conclusions

In this study we investigate the feasibility of discriminating the mass composition of cosmic rays at PeV energies by utilizing the LCm parameter, which measures the signal non-uniformity recorded in detectors placed at a specific distance from the shower core at ground level.

Our analysis based on Monte Carlo simulations using the KASCADE array revealed that the LCm parameter is minimally dependent on the specific hadronic interaction model at high energies considered: QGSjet-II-02, QGSjet-II-04, EPOS-LHC, SIBYLL 2.3c and SIBYLL 2.3d.

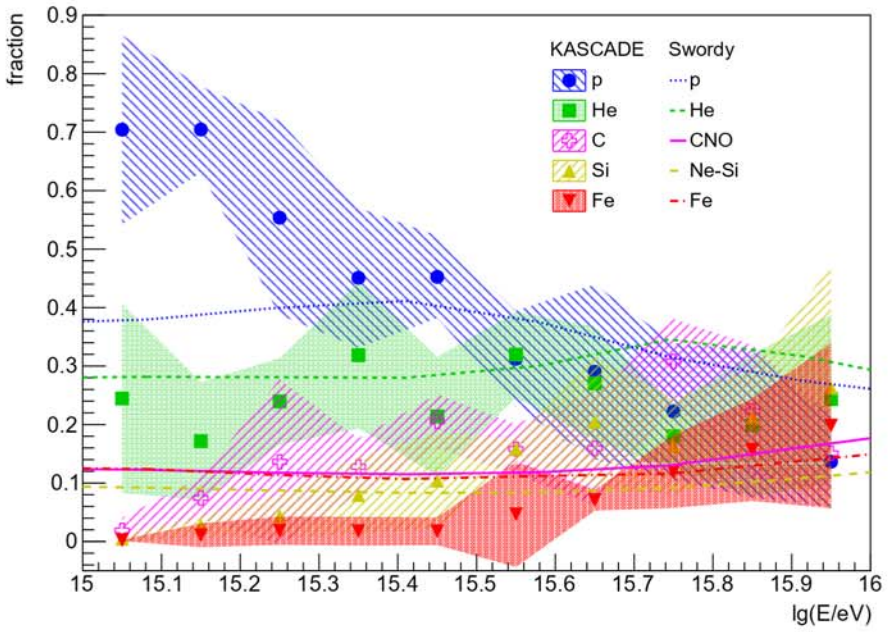

Figure 10. Evolution of the individual fractions of nuclei obtained in this work as a function of primary energy, in comparison with predictions of the astrophysical model proposed by Swordy [44]. The error bands represent the standard deviation of the individual fractions obtained from all five hadronic interaction models used in this work.

Furthermore, we performed a mass composition analysis using data collected by the KASCADE experiment in the energy range $\lg(E/\mathrm{eV}) = [15.0 - 16.0]$ around the *knee*, with the LCm parameter obtained from Monte Carlo simulations for five primary species (p, He, C, Si, and Fe). Our results indicated a linear decrease in the abundance of protons with increasing energy, while the heavier components became dominant above the knee, in agreement with the predictions of all five hadronic interaction models.

We also found that our results qualitatively support three astrophysical models that relate the origin of the *knee* in the energy spectrum with different acceleration and propagation scenarios [43–45]. The observed evolutionary trend of each primary abundance of the various types of particles with respect to energy is consistent with the predictions of these models.

Based on these results, we conclude that the LCm parameter can effectively serve as a model-independent discriminator for mass composition studies at PeV energies in experiments that use a relatively compact array of detectors.

Acknowledgments

I am grateful to the KCDC team who made possible the access to data and simulations of the KASCADE experiment, especially to Jürgen Wochele for the assistance provided in accessing the data. I also would like to thank Ionel Lazanu and Mihaela Parvu for carefully reading the manuscript and providing useful comments.

This research was supported by Romanian Ministry of Research, Innovation and Digitalization under Romanian National Core Program LAPLAS VII - contract no. 30N/2023.

References

[1] T. Antoni *et al.* [KASCADE], "KASCADE measurements of energy spectra for elemental groups of cosmic rays: Results and open problems," Astropart. Phys. **24**, 1-25 (2005) doi:10.1016/j.astropartphys.2005.04.001 [arXiv:astro-ph/0505413 [astro-ph]].

[2] M. Takeda, N. Sakaki, K. Honda, M. Chikawa, M. Fukushima, N. Hayashida, N. Inoue, K. Kadota, F. Kakimoto and K. Kamata, *et al.* "Energy determination in the Akeno Giant Air Shower Array experiment," Astropart. Phys. **19**, 447-462 (2003) doi:10.1016/S0927-6505(02)00243-8 [arXiv:astro-ph/0209422 [astro-ph]].

[3] M. Nagano, T. Hara, Y. Hatano, N. Hayashida, S. Kawaguchi, K. Kamata, T. Kifune and Y. Mizumoto, "Energy Spectrum of Primary Cosmic Rays Between 10**14.5-ev and 10**18-ev," J. Phys. G **10**, 1295 (1984) doi:10.1088/0305-4616/10/9/016

[4] S. Ogio, F. Kakimoto, Y. Kurashina, O. Burgoa, D. Harada, H. Tokuno, H. Yoshii, A. Morizawa, E. Gotoh and H. Nakatani, *et al.* "The energy spectrum and the chemical composition of primary cosmic rays with energies from 10**14-eV to 10**16-eV," Astrophys. J. **612**, 268-275 (2004) doi:10.1086/422510

[5] J. W. Fowler, L. F. Fortson, C. C. H. Jui, D. B. Kieda, R. A. Ong, C. L. Pryke and P. Sommers, "A Measurement of the cosmic ray spectrum and composition at the knee," Astropart. Phys. **15**, 49-64 (2001) doi:10.1016/S0927-6505(00)00139-0 [arXiv:astro-ph/0003190 [astro-ph]].

[6] M. A. K. Glasmacher, M. A. Catanese, M. C. Chantell, C. E. Covault, J. W. Cronin, B. E. Fick, L. F. Fortson, J. W. Fowler, K. D. Green and D. B. Kieda, *et al.* Astropart. Phys. **10**, 291-302 (1999) doi:10.1016/S0927-6505(98)00070-X

[7] S. P. Swordy and D. B. Kieda, "Elemental composition of cosmic rays near the knee by multiparameter measurements of air showers," Astropart. Phys. **13**, 137-150 (2000) doi:10.1016/S0927-6505(99)00117-6 [arXiv:astro-ph/9909381 [astro-ph]].

[8] M. Aglietta *et al.* [EAS-TOP], "The EAS size spectrum and the cosmic ray energy spectrum in the region 10**15-eV - 10**16-eV," Astropart. Phys. **10**, 1-9 (1999) doi:10.1016/S0927-6505(98)00035-8

[9] W. D. Apel *et al.* [KASCADE Grande], "Kneelike structure in the spectrum of the heavy component of cosmic rays observed with KASCADE-Grande," Phys. Rev. Lett. **107**, 171104 (2011) doi:10.1103/PhysRevLett.107.171104 [arXiv:1107.5885 [astro-ph.HE]].

[10] M. G. Aartsen *et al.* [IceCube], Phys. Rev. D **100**, no.8, 082002 (2019) doi:10.1103/PhysRevD.100.082002 [arXiv:1906.04317 [astro-ph.HE]].

[11] R. U. Abbasi *et al.* [Telescope Array], Astrophys. J. **865**, no.1, 74 (2018) doi:10.3847/1538-4357/aada05 [arXiv:1803.01288 [astro-ph.HE]].

[12] O. Deligny [Pierre Auger and Telescope Array], "The energy spectrum of ultra-high energy cosmic rays measured at the Pierre Auger Observatory and at the Telescope Array," PoS **ICRC2019**, 234 (2020) doi:10.22323/1.358.0234 [arXiv:2001.08811 [astro-ph.HE]].

[13] P. Abreu *et al.* [Pierre Auger], "The energy spectrum of cosmic rays beyond the turn-down around 10^{17} eV as measured with the surface detector of the Pierre Auger Observatory," Eur. Phys. J. C **81**, no.11, 966 (2021) doi:10.1140/epjc/s10052-021-09700-w [arXiv:2109.13400 [astro-ph.HE]].

[14] A. Aab *et al.* [Pierre Auger], "Features of the Energy Spectrum of Cosmic Rays above 2.5×10^{18} eV Using the Pierre Auger Observatory," Phys. Rev. Lett. **125**, no.12, 121106 (2020) doi:10.1103/PhysRevLett.125.121106 [arXiv:2008.06488 [astro-ph.HE]].

[15] R. U. Abbasi *et al.* [Telescope Array], "The energy spectrum of cosmic rays above $10^{17.2}$ eV measured by the fluorescence detectors of the Telescope Array experiment in seven years," Astropart. Phys. **80**, 131-140 (2016) doi:10.1016/j.astropartphys.2016.04.002 [arXiv:1511.07510 [astro-ph.HE]].

[16] T. Stanev, P. L. Biermann and T. K. Gaisser, "Cosmic rays. 4. The Spectrum and chemical composition above 10**4-GeV," Astron. Astrophys. **274**, 902 (1993) [arXiv:astro-ph/9303006 [astro-ph]].

[17] E. Roulet, "Astroparticle theory: some new insights into high energy cosmic rays," Int. J. Mod. Phys. A **19**, 1133-1141 (2004) doi:10.1142/S0217751X04019044 [arXiv:astro-ph/0310367 [astro-ph]].

[18] S. Karakula and W. Tkaczyk, "The formation of the cosmic ray energy spectrum by a photon field," Astropart. Phys. **1**, 229-237 (1993) doi:10.1016/0927-6505(93)90023-7

[19] J. R. Hörandel, "Models of the knee in the energy spectrum of cosmic rays," Astropart. Phys. **21**, 241-265 (2004) doi:10.1016/j.astropartphys.2004.01.004 [arXiv:astro-ph/0402356 [astro-ph]].

[20] M. Amenomori et al. (Tibet ASgamma Collaboration), "First Detection of sub-PeV Diffuse Gamma Rays from the Galactic Disk: Evidence for Ubiquitous Galactic Cosmic Rays beyond PeV Energies," Phys. Rev. Lett. **126**, 141101 (2021), doi: 10.1103/PhysRevLett.126.141101, arXiv:2104.05181 [astro-ph.HE].

[21] Zhen Cao et al., "Ultrahigh-energy photons up to 1.4 petaelectronvolts from 12 γ ray Galactic sources," Nature **594**, 33-36 (2021), doi: 10.1038/s41586-021-03498-z.

[22] J. R. Hörandel, "A Review of experimental results at the knee," J. Phys. Conf. Ser. **47**, 41-50 (2006) doi:10.1088/1742-6596/47/1/005 [arXiv:astro-ph/0508014 [astro-ph]].

[23] K. H. Kampert *et al.* [KASCADE], "Cosmic ray energy spectra and mass composition at the knee - Recent results from KASCADE," Nucl. Phys. B Proc. Suppl. **136**, 273-281 (2004) doi:10.1016/j.nuclphysbps.2004.10.035 [arXiv:astro-ph/0410559 [astro-ph]].

[24] A. Haungs, "Energy spectrum and mass composition around the knee by EAS measurements," J. Phys. G **29**, 809-820 (2003) doi:10.1088/0954-3899/29/5/303 [arXiv:astro-ph/0212481 [astro-ph]].

[25] R. Conceição, L. Gibilisco, M. Pimenta and B. Tomé, "Gamma/hadron discrimination at high energies through the azimuthal fluctuations of air shower particle distributions at the ground," JCAP **10**, 086 (2022) doi:10.1088/1475-7516/2022/10/086 [arXiv:2204.12337 [hep-ph]].

[26] T. Antoni *et al.* [KASCADE], "The Cosmic ray experiment KASCADE," Nucl. Instrum. Meth. A **513**, 490-510 (2003) doi:10.1016/S0168-9002(03)02076-X

[27] A. Haungs, D. Kang, S. Schoo, D. Wochele, J. Wochele, W. D. Apel, J. C. Arteaga-Velázquez, K. Bekk, M. Bertaina and J. Blümer, *et al.* "The KASCADE Cosmic-ray Data Centre KCDC: Granting Open Access to Astroparticle Physics Research Data," Eur. Phys. J. C **78**, no.9, 741 (2018) doi:10.1140/epjc/s10052-018-6221-2 [arXiv:1806.05493 [astro-ph.IM]].

[28] J. Wochele, D. Kang, D. Wochele, A. Haungs and S. Schoo, "KCDC User Manual," doi:http://doi.org/10.17616/R3TS4P, V.2.3, 2022-05-09.

[29] J. Wochele, D. Kang, D. Wochele, A. Haungs and S. Schoo, "KCDC Simulation Manual - KASCADE, GRANDE and CALORIMETER Simulations," http://doi.org/10.17616/R3TS4P, V.02.2, 2022-05-04.

[30] D. Heck and J. Knapp, *Report* **FZKA 6097** *(1998), Forschungszentrum Karlsruhe; available from http://www-ik.fzk.de/~heck/publications/*, 1989.

[31] D. Heck and J. Knapp and J.N. Capdevielle and G. Schatz and T. Thouw, *Report* **FZKA 6019** *(1998), Forschungszentrum Karlsruhe; available from http://www-ik.fzk.de/corsika/physics_description/corsika_phys.html* , 1998.

[32] R. Brun, F. Bruyant, M. Maire, A. C. McPherson and P. Zanarini, "GEANT3," CERN-DD-EE-84-1.

[33] A. Haungs, D. Kang, S. Schoo, D. Wochele, J. Wochele, W. D. Apel, J. C. Arteaga-Velázquez, K. Bekk, M. Bertaina and J. Blümer, *et al.* "The KASCADE Cosmic-ray Data Centre KCDC: Granting Open Access to Astroparticle Physics Research Data," Eur. Phys. J. C **78**, no.9, 741 (2018) doi:10.1140/epjc/s10052-018-6221-2 [arXiv:1806.05493 [astro-ph.IM]].

[34] S. Ostapchenko, "QGSJET-II: Towards reliable description of very high energy hadronic interactions," Nucl. Phys. B Proc. Suppl. **151**, 143-146 (2006) doi:10.1016/j.nuclphysbps.2005.07.026 [arXiv:hep-ph/0412332 [hep-ph]].

[35] T. Pierog, I. Karpenko, J. M. Katzy, E. Yatsenko and K. Werner, "EPOS LHC: Test of collective hadronization with data measured at the CERN Large Hadron Collider," Phys. Rev. C **92**, no.3, 034906 (2015) doi:10.1103/PhysRevC.92.034906 [arXiv:1306.0121 [hep-ph]].

[36] A. Fedynitch, F. Riehn, R. Engel, T. K. Gaisser and T. Stanev, "Hadronic interaction model sibyll 2.3c and inclusive lepton fluxes," Phys. Rev. D **100**, no.10, 103018 (2019) doi:10.1103/PhysRevD.100.103018 [arXiv:1806.04140 [hep-ph]].

[37] F. Riehn, R. Engel, A. Fedynitch, T. K. Gaisser and T. Stanev, "Hadronic interaction model Sibyll 2.3d and extensive air showers," Phys. Rev. D **102**, no.6, 063002 (2020) doi:10.1103/PhysRevD.102.063002 [arXiv:1912.03300 [hep-ph]].

[38] A. Ferrari, Paola R. Sala, A. Fassò, and Johannes Ranft. *FLUKA: A multi-particle transport code (program version 2005)*. Geneva: CERN, 2005. https://cds.cern.ch/record/898301.

[39] O. Sima, H. Rebel, A. Haungs, G. Toma, C. Manailescu, C. Morariu, J. C. Arteaga, K. Bekk, M. Bertaina and J. Blumer, *et al.* "Restoring the azimuthal symmetry of lateral distributions of charged particles in the range of the KASCADE-Grande experiment," Nucl. Instrum. Meth. A **638**, 147-156 (2011) doi:10.1016/j.nima.2011.02.069

[40] T. Antoni *et al.* [KASCADE], "The Cosmic ray experiment KASCADE," Nucl. Instrum. Meth. A **513**, 490-510 (2003) doi:10.1016/S0168-9002(03)02076-X

[41] G. Di Sciascio, "The LHAASO experiment: From Gamma-Ray Astronomy to Cosmic Rays," *Nuclear and Particle Physics Proceedings*, vol. 279-281, pp. 166-173, 2016. Proceedings of the 9th Cosmic Ray International Seminar. ISSN: 2405-6014. DOI: https://doi.org/10.1016/j.nuclphysbps.2016.10.024.

[42] W. D. Apel [KASCADE], "Energy Spectra of Elemental Groups of Cosmic Rays: Update on the KASCADE Unfolding Analysis," Astropart. Phys. **31**, 86-91 (2009) doi:10.1016/j.astropartphys.2008.11.008 [arXiv:0812.0322 [astro-ph]].

[43] R. Plaga, "A possible universal origin of hadronic cosmic rays from ultrarelativistic ejecta of bipolar supernovae," New Astron. **7**, 317-336 (2002) doi:10.1016/S1384-1076(02)00135-5 [arXiv:astro-ph/0106033 [astro-ph]].

[44] S.P. Swordy, *Proc. 24th Int. Cosmic Ray Conf.*, Rome 2, 697 (1995).

[45] L. G. Sveshnikova, "The knee in galactic cosmic ray spectrum and variety in supernovae," Astron. Astrophys. **409**, 799-808 (2003) doi:10.1051/0004-6361:20030909 [arXiv:astro-ph/0303159 [astro-ph]].

[46] X. Zuo *et al.* [LHAASO], "Design and performances of prototype muon detectors of LHAASO-KM2A," Nucl. Instrum. Meth. A **789**, 143-149 (2015) doi:10.1016/j.nima.2015.04.010.

[47] F. Aharonian *et al.* [LHAASO], "Self-calibration of LHAASO-KM2A electromagnetic particle detectors using single particles within extensive air showers," Phys. Rev. D **106**, no.12, 122004 (2022) doi:10.1103/PhysRevD.106.122004.